

Comparing Minimal and Non-Minimal Quintessence Models to 2025 DESI Data

Husam Adam^{1a}, Mark P. Hertzberg^{1,2b}, Daniel Jiménez-Aguilar^{1c}, Iman Khan^{1,3d}

¹*Institute of Cosmology, Department of Physics and Astronomy,
Tufts University, Medford, MA 02155, USA*

²*Institute of Advanced Study, Hong Kong University
of Science and Technology, Hong Kong and*

³*Beloit College, Beloit, WI 53511, USA*

Abstract

In this work we examine the 2025 DESI analysis of dark energy, which suggests that dark energy is evolving in time with an increasing equation of state w . We explore a wide range of quintessence models, described by a potential function $V(\varphi)$, including: quadratic potentials, quartic hilltops, double wells, cosine functions, Gaussians, inverse powers. We find that while some provide improvement in fitting to the data, compared to a cosmological constant, the improvement is only modest. We then consider non-minimally coupled scalars which can help fit the data by providing an effective equation of state that temporarily obeys $w < -1$ and then relaxes to $w > -1$. Since the scalar is very light, this leads to a fifth force and to time evolution in the effective gravitational strength, which are both tightly constrained by tests of gravity. For a very narrow range of carefully selected non-minimal couplings we are able to evade these bounds, but not for generic values.

^a Husam.Adam@tufts.edu

^b mark.hertzberg@tufts.edu

^c Daniel.Jimenez_Aguilar@tufts.edu

^d khani@beloit.edu

CONTENTS

I. Introduction	3
II. Models	5
A. Potentials	5
1. Hilltop Potentials	6
2. Monomial Potentials	9
3. Decaying Potentials	9
III. Statistical Analysis	12
IV. Non-Minimal Coupling	13
A. Fifth Force Constraints	14
B. Gravitational Coupling Constraints	15
C. Choice of Frame	15
D. Results	16
V. Discussion	21
VI. Acknowledgments	21
References	22

I. INTRODUCTION

The accelerated expansion of the universe [1, 2] is attributed to the presence of dark energy, which is characterized by an equation of state $w_{\text{DE}} = p_{\text{DE}}/\rho_{\text{DE}} < -1/3$ and constitutes, approximately, 69% of the total energy density in the universe. Despite the fact that the magnitude-redshift data for type IA supernovae and the analysis of the temperature fluctuations in the Cosmic Microwave Background (CMB) strongly suggest the existence of dark energy, a fundamental description of it is still lacking. The simplest approach is to describe it as a cosmological constant, often referred to as Λ . In this case, the dark energy density remains constant in time throughout the history of the universe, with equation of state $w_{\Lambda} = -1$. Although this model (dubbed Λ CDM) has been successful in explaining the observational data until now, it requires an energy density of $\rho_{\Lambda} \sim 10^{-47} \text{ GeV}^4$, which is in large tension with the expected vacuum energy in the framework of Quantum Field Theory. This discrepancy (which is 122 orders of magnitude if compared to the Planck density), is known as the cosmological constant problem [3], which we will not attempt to solve in this work.

The Λ CDM paradigm is arguably in tension with recent results from the Dark Energy Spectroscopic Instrument (DESI) collaboration, which has reported evidence for a time-evolving dark energy density [4, 5]. The survey combines Baryon Acoustic Oscillation (BAO) and CMB measurements, as well as three different sets of type Ia Supernovae (Sne Ia) data: Pantheon+, Union3 and DESY5. The analysis performed for each of them in the latest release indicates 2.8σ , 3.8σ and 4.2σ tensions with the Λ CDM model, respectively. The DESI collaboration described the dynamical dark energy equation of state with the so-called Chevallier-Polarski-Linder (CPL) parametrization [6, 7]:

$$w_{\text{DE}}(a) = w_0 + (1 - a)w_a, \quad (1)$$

where a is the scale factor and the parameters w_0 and w_a denote the equation of state and its derivative today ($a=1$). Note that the cosmological constant is obtained for $w_0 = -1$ and $w_a = 0$. While the CPL parametrization is by no means fundamental or generic, it might be a good approximation in the range of redshifts¹ to which DESI is sensitive ($0.295 \leq z \leq 2.33$). Other alternatives and extensions of the CPL parametrization have also been discussed in the literature (see, for instance, [8–15]).

There is a wide variety of models that can describe dynamical dark energy. The simplest ones are canonical quintessence models, where the role of dark energy is played by a scalar field φ (with standard kinetic structure and minimal coupling to gravity) that evolves

¹ Redshift is related to the scale factor via $z = -1 + 1/a$.

under the influence of some potential $V(\varphi)$. However, one can anticipate that this class of theories may not be the best candidates to provide an excellent fit to the DESI data. According to DESI's results, the central values of the CPL parameters are $w_{0,\text{central}} \approx -0.7$ and $w_{a,\text{central}} \approx -1$, and so $w_{\text{DE,central}}(a) \approx -1.7 + a$. Therefore, if we were to extrapolate the CPL parametrization all the way to the past, we would find $w_{\text{DE}} < -1$ for $a < 0.7$, or in other words, for $z > 0.43$. This means that the Null Energy Condition (NEC) would be violated for such redshifts, but this cannot happen for minimally coupled scalar fields with canonical kinetic terms.² Since $z = 0.43$ lies inside DESI's range of redshifts, one concludes that an accurate fit to the DESI data is not possible, although there could still be a modest level of compatibility.³ Values of w_0 and w_a closer to the central ones may be obtained in theories where NEC violation is not forbidden (or is just apparent). These include models of scalar fields non-minimally coupled to gravity [18–21] (see also [22, 23]), braneworld dark energy [24], dark matter-dark energy interactions [25–30] (see [31] for a detailed review), fields with non-standard kinetic terms [32, 33] or modified gravity theories [34–39]. Other possibilities are based on non-standard equations of state for dark matter [40–42] and modified cosmologies in the framework of holographic dark energy [43] or the generalized uncertainty principle [44]. To date, the strongest evidence for a phantom crossing in the equation of state of dark energy has been reported in [45] with an approximate significance level of 5σ .

In this paper, we will extend the work presented in [46] for other quintessence potentials, and we will also consider scalar field models with a non-minimal coupling to gravity. Our goal is to assess whether the DESI data significantly favors these theories over the ΛCDM model.

The manuscript is structured as follows. We study a set of canonical quintessence models characterized by different scalar potentials in Sec. II, and provide their statistical analysis in Sec. III. Then, in Sec. IV, we report on our findings for scalar fields non-minimally coupled to gravity. Finally, we present our conclusions in Sec. V.

We work in natural units ($c = \hbar = 1$) and use the $(- +++)$ convention for the spacetime metric. Furthermore, M_p will denote the reduced Planck mass: $M_p = 1/\sqrt{8\pi G}$.

² The equation of state parameter can be written as $w_{\text{DE}} = -1 + (p_\varphi + \rho_\varphi)/\rho_\varphi$. The NEC states that $p_\varphi + \rho_\varphi > 0$, and thus $w_{\text{DE}} > -1$. For a minimally coupled scalar field, this is always true as $p_\varphi + \rho_\varphi = \dot{\varphi}^2$.

However, we can relax this for non-minimally coupled scalars, as we discuss later.

³ In models that consider an extended parameter space, this level of compatibility can be higher (see, for instance, [16, 17]).

II. MODELS

We start by considering canonical quintessence models in which a single scalar field φ plays the role of the dark energy. These models are described by the following action:

$$S = \int d^4x \sqrt{-g} \left[\frac{M_p^2}{2} R - \frac{1}{2} g^{\mu\nu} \partial_\mu \varphi \partial_\nu \varphi - V(\varphi) + \mathcal{L}_m \right], \quad (2)$$

where R is the Ricci scalar, $V(\varphi)$ is the potential energy density of the scalar field and \mathcal{L}_m denotes the Lagrangian density of the matter fields.

Focussing on an FLRW universe, the equation of motion for the scalar field reads

$$\ddot{\varphi} + 3H\dot{\varphi} + V'(\varphi) = 0. \quad (3)$$

Moreover, the evolution of the scale factor is governed by the Friedmann equation:

$$H^2 = \frac{1}{3M_p^2} (\rho_m + \rho_\varphi), \quad (4)$$

where $H = \dot{a}/a$ is the Hubble rate and ρ_m and ρ_φ respectively denote the energy densities of matter (proportional to a^{-3}) and the scalar field. The latter is given by

$$\rho_\varphi = \frac{\dot{\varphi}^2}{2} + V(\varphi). \quad (5)$$

Since we are mostly interested in late-time dynamics, we are neglecting the contribution of radiation. Note also that we are considering a spatially flat universe.

In the following subsections, we numerically solve (3) and (4) for different scalar field potentials. Regarding the initial conditions, the field will be released from rest⁴ ($\dot{\varphi}_i = 0$) at different values φ_i . This completely determines the initial energy density of the scalar field. On the other hand, the initial energy density of matter will be chosen to be much greater than that of the scalar field.

A. Potentials

The quintessence models are specified by a potential $V(\varphi)$. Since φ is a Lorentz scalar, so is any function $V(\varphi)$. Hence there are infinitely many options for the potential. To make progress, we will consider a range of potential functions. Those considered in this work are shown in Fig. 1.

For each value of φ_i and parameters in the potential we evolve the system. We then output the equation of state w , and take its best fit value between redshifts $0.295 \leq z \leq 2.33$. The procedure is indicated in Fig. 2 for the upcoming case of the linear potential.

⁴ We will assume that the initial Hubble rate is high enough to keep the field frozen at early times. Later when we study non-minimally coupled models, this is more subtle.

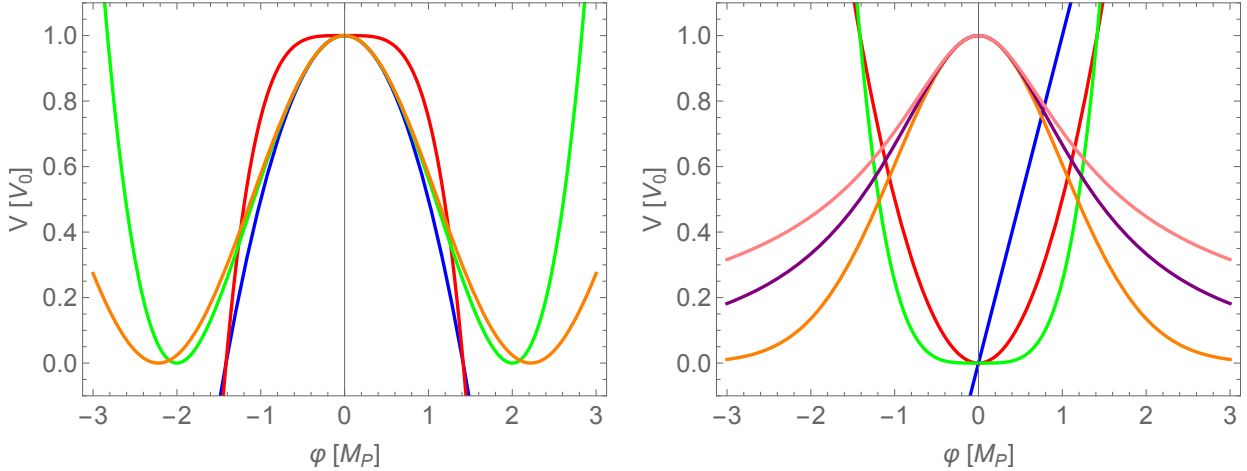


FIG. 1. Potentials $V(\varphi)$ considered in this work. Left: Blue is quadratic hilltop eq. (6), red is quartic hilltop eq. (7), green is double well with $\lambda = 1$ eq. (8), orange is cosine eq. (9). Right: Blue is linear monomial eq. (10), red is quadratic monomial eq. (11), green is quartic monomial eq. (12), orange is Gaussian eq. (13), purple is inverse function eq. (14), pink is inverse square root function eq. (15). We have set $k = 1$ throughout.

1. Hilltop Potentials

In Ref. [46] there was a focus on models near a hilltop, in which the potential is a constant minus a quadratic. We will reexamine this here (eq. (6)) in light of the updated 2025 DESI data. Moreover, we will also consider a range of other hilltop potentials: a quartic hilltop (eq. (7)), as well as models with local minima (eqs. (8,9)). For the double well in eq. (8), it has a late-time vacuum energy that vanishes if $\lambda = 1$, but is non-zero otherwise. We note that since these models all have dynamical dark energy, we will not need to run them to very late times; so it is not directly important if the (very) late time vacuum energy is positive, negative, or vanishing. The set of potentials considered is:

$$V(\varphi) = V_0 \left(1 - \frac{k^2}{2M_p^2} \varphi^2 \right) \quad (6)$$

$$V(\varphi) = V_0 \left(1 - \frac{k^4}{4M_p^4} \varphi^4 \right) \quad (7)$$

$$V(\varphi) = V_0 \left(1 - \frac{k^2}{2M_p^2} \varphi^2 + \frac{\lambda k^4}{16M_p^4} \varphi^4 \right) \quad (8)$$

$$V(\varphi) = \frac{V_0}{2} \left(1 + \cos \left(\frac{\sqrt{2} k \varphi}{M_p} \right) \right) \quad (9)$$

Here, the overall scale that sets the density V_0 will be rewritten in terms of a characteristic mass scale m via $V_0 = m^2 M_p^2$. Going forwards, we will measure time in units of m^{-1} .

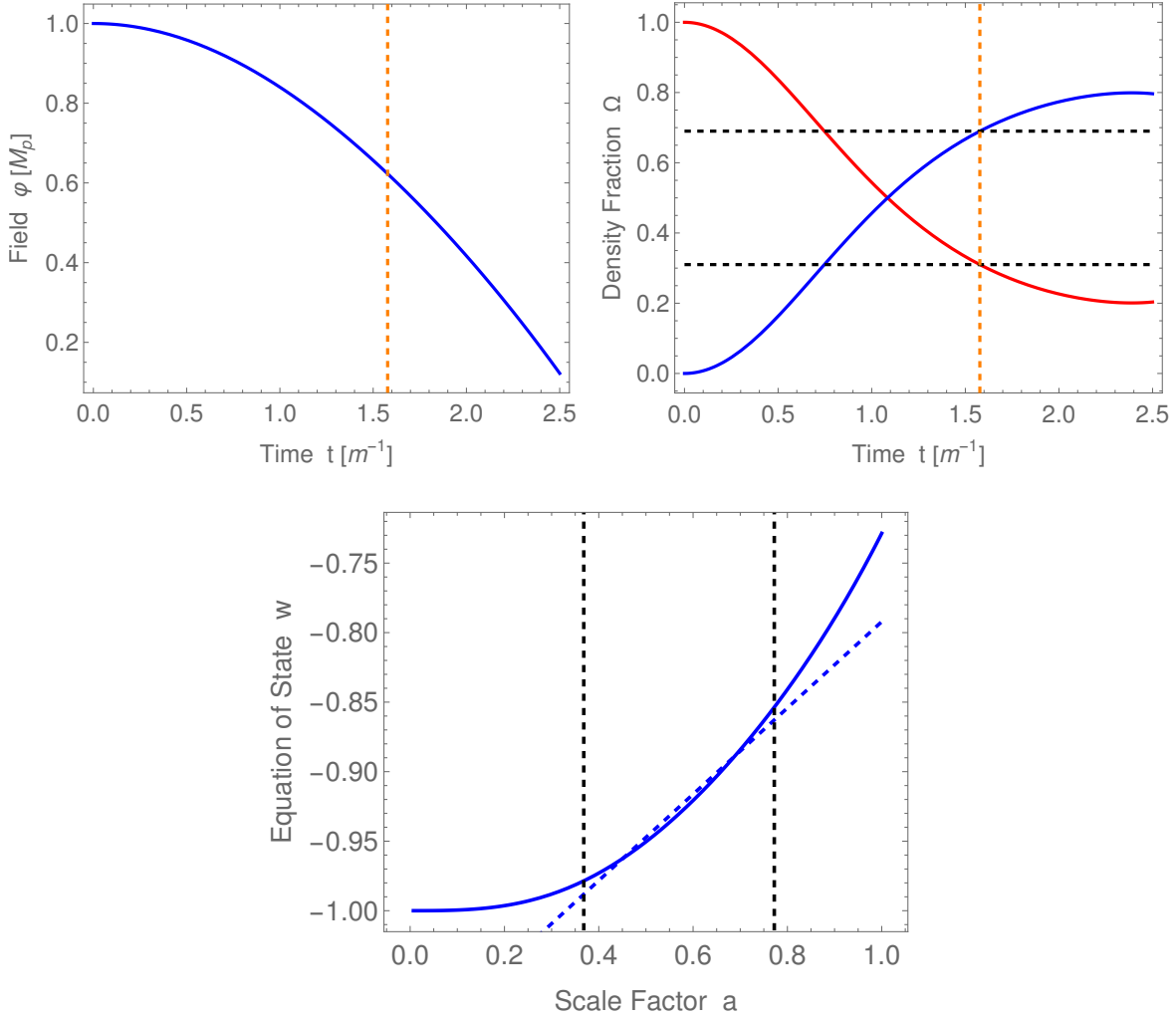


FIG. 2. Top left: Value of the scalar field as a function of time. Top right: Fractional energy densities of matter (red) and dark energy (blue). The vertical dashed line (orange) corresponds to the current time, defined as the moment at which the dark energy density fraction becomes $\Omega_{DE,0} = 0.69$, which in this case is $t_0 \approx 1.58m^{-1}$. Bottom: Dark energy equation of state w as a function of the scale factor (solid curve) and CPL fit (blue dashed line). The vertical lines indicate the range over which DESI is most sensitive. The present time is at $a = 1$. These plots are for the linear potential eq. (10) with $\varphi_i = M_p$.

These potentials are expressed in terms of a dimensionless parameter k , which controls the curvature at the hilltop. For $k \ll 1$, the field rolls very slowly off the hilltop. For $k \gg 1$, the field rolls very quickly off the hilltop. In the latter case, to have a long-lived universe, one should have the field begin very close to the hilltop, so this still takes quite some time.

Taking the values from the best fit for w_0 , w_a , we report our results for this set of models in Fig. 3. Each curve is for a fixed value of k , with φ_i varied. For $\varphi_i \rightarrow 0$, the field is sitting

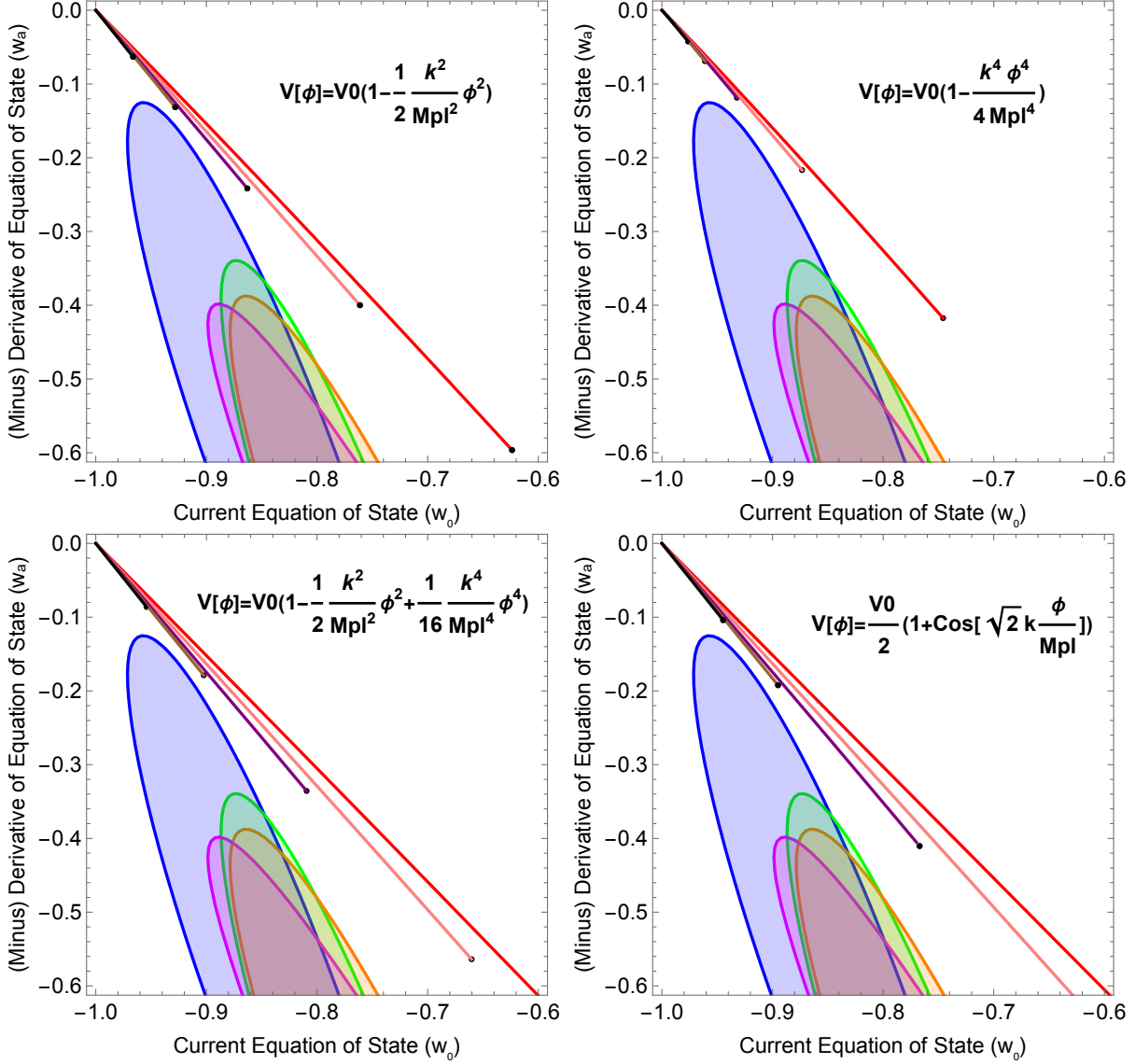


FIG. 3. Equation of state parameters w_a versus w_0 . Top left is quadratic hilltop potential eq. (6). Top right is quartic hilltop potential eq. (7). Bottom left is double well potential with $\lambda = 1$ eq. (8). Bottom right is cosine potential eq. (9). Red is $k = 1$, pink is $k = 2$, purple is $k = 3$, brown is $k = 4$, and black is $k = 5$. We are varying φ_i up to its maximum value. Also, the three different contours correspond approximately to the 95% region of the datasets DESI BAO + CMB + PantheonPlus (blue), DESI BAO + CMB + Union3 (orange), DESI BAO + CMB + DESY5 (green), and DESI BAO + CMB (magenta) from Ref. [5].

extremely close to the hilltop and so it acts as a cosmological constant ($w_0 = -1$, $w_a = 0$), while for larger φ_i it becomes dynamical. There is typically a maximum value for φ_i ; beyond this, the field rolls so fast that the dark energy density never grows to be $\Omega_{DE,0} = 0.69$. So we end the curves at these points (this is indicated by the dots at the ends of the lines).

Overall we see that all the curves do not go through the data; though some get close.

2. Monomial Potentials

We also consider models which are a pure (positive) power law – a monomial. If the field starts near the minimum, then it just oscillates for even powers or becomes negative for odd powers, and does not act as dark energy at all. So there is a minimum value of φ_i here. For the linear potential it is $\varphi_{\min,i} \approx 0.85M_p$; for the quadratic monomial it is $\varphi_{\min,i} \approx 1.4M_p$; for the quartic monomial it is $\varphi_{\min,i} \approx 2.4M_p$. On the other hand, if the field starts at $\varphi_i \gg M_p$, then the evolution is similar to that of a cosmological constant. So the intermediate regime in which $\varphi_i \sim \text{few} \times M_p$ is of most interest for dynamical dark energy. The power laws considered in this work are:

$$V(\varphi) = V_0 \left(\frac{\varphi}{M_p} \right) \quad (10)$$

$$V(\varphi) = \frac{V_0}{2} \left(\frac{\varphi}{M_p} \right)^2 \quad (11)$$

$$V(\varphi) = \frac{V_0}{4} \left(\frac{\varphi}{M_p} \right)^4 \quad (12)$$

By measuring time in units of m^{-1} (recall $V_0 = m^2 M_p^2$), the only remaining parameter in these models is the initial φ_i (in units of M_p). The results for this analysis are given in Fig. 4. We note that in this case, both the pure quadratic and the pure quartic give rather similar results. And none of the results really cuts into the DESI data.

3. Decaying Potentials

Another family of potentials we consider are those that decay asymptotically towards $V \rightarrow 0$ at large φ . For small φ , these are similar to the hilltop models considered earlier. However, for large φ , there is a new type of behavior. In eq. (13) there is rapid decay from a Gaussian. In eq. (14) there is inverse power law decay. In eq. (15) there is inverse square root decay. The potentials are:

$$V(\varphi) = V_0 \exp \left(-\frac{k^2 \varphi^2}{2M_p^2} \right) \quad (13)$$

$$V(\varphi) = V_0 \left(1 + \frac{k^2 \varphi^2}{2M_p^2} \right)^{-1} \quad (14)$$

$$V(\varphi) = V_0 \left(1 + \frac{k^2 \varphi^2}{M_p^2} \right)^{-1/2} \quad (15)$$

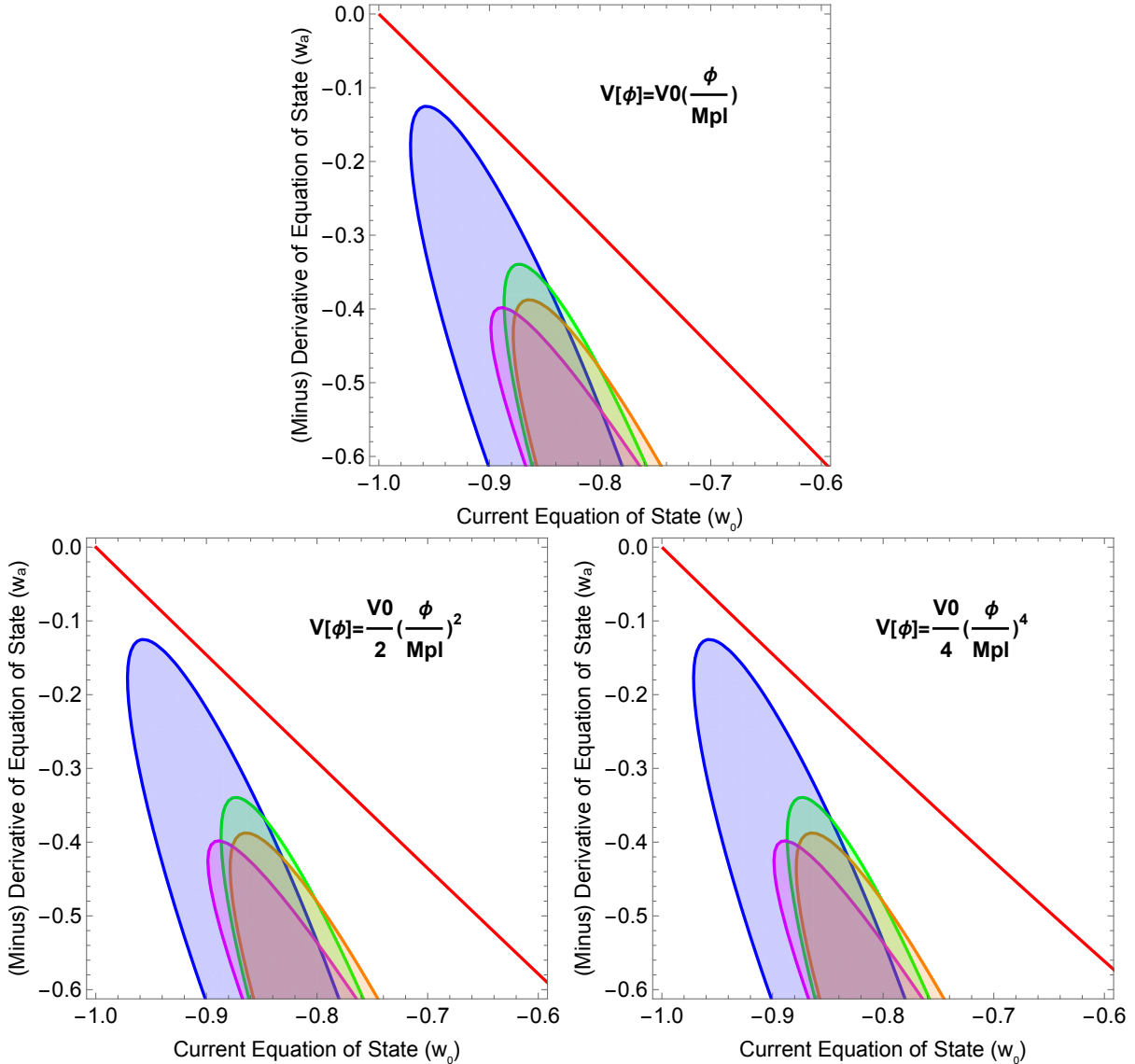


FIG. 4. Equation of state parameters w_a versus w_0 . Top is pure linear potential eq. (10). Left is pure quadratic potential eq. (11). Right is pure quartic potential eq. (12). We are varying φ_i from its minimum value. Also, the three different contours correspond approximately to the 95% region of the datasets DESI BAO + CMB + PantheonPlus (blue), DESI BAO + CMB + Union3 (orange), DESI BAO + CMB + DESY5 (green), and DESI BAO + CMB (magenta) from Ref. [5].

We note that in the power law decay cases, there is qualitatively new behavior at large φ . The results in the w_0, w_a plane are given in Fig. 5. At large φ we see that the shape of the curves turn around. This is because there are now two limits in which we have a cosmological constant: small φ_i and large φ_i . We see that the turn-around is in the wrong direction relative to the data, so the fit is still not accurate. But going forward, we wish to be precise.

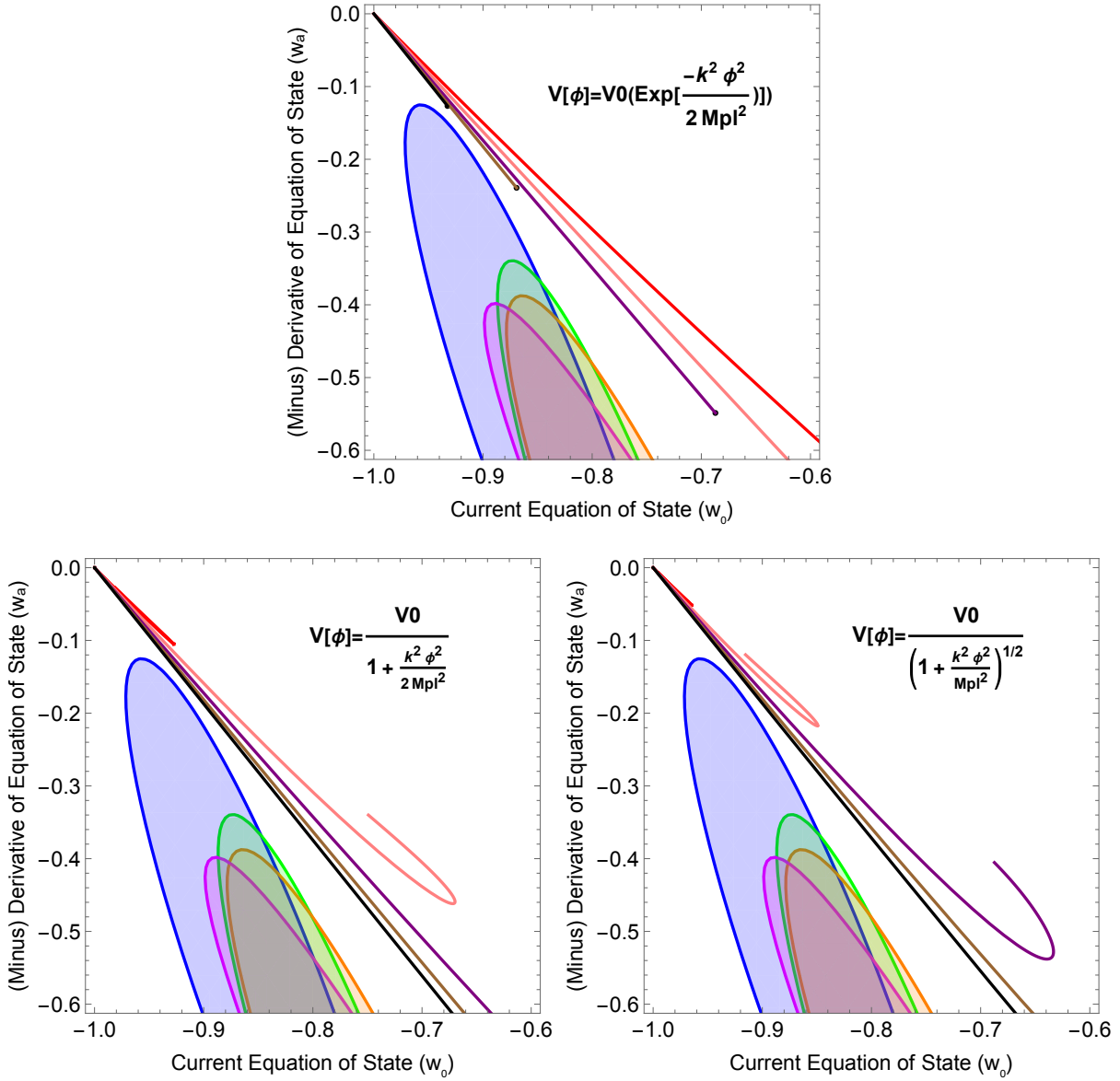


FIG. 5. Equation of state parameters w_a versus w_0 . Top is Gaussian potential eq. (13). Bottom left is inverse potential eq. (14). Bottom right is inverse square root potential eq. (15). Red is $k = 1$, pink is $k = 2$, purple is $k = 3$, brown is $k = 4$, and black is $k = 5$. We are varying φ_i to large values. The inverse potentials continue to loop around to the cosmological constant point. Also, the three different contours correspond approximately to the 95% region of the datasets DESI BAO + CMB + PantheonPlus (blue), DESI BAO + CMB + Union3 (orange), DESI BAO + CMB + DESY5 (green), and DESI BAO + CMB (magenta) from Ref. [5].

III. STATISTICAL ANALYSIS

In order to assess the statistical preference for the quintessence models described above, we follow the procedure described in Ref. [46]. Firstly, the joint probability density function of w_0 and w_a is assumed to be Gaussian:

$$P(w_0, w_a) \propto \exp(-c_1 w_0^2 - c_2 w_a^2 - c_3 w_0 w_a - c_4 w_0 - c_5 w_a), \quad (16)$$

where the c_i coefficients depend on the specific supernovae data set (Pantheon+, Union3 or DESY5) and can be calculated once we extract the equations for the constant-density contours presented in the latest DESI release [5]. Consider now a concrete quintessence model (for instance, the quadratic hilltop potential with $k = 1$). For every initial value of the field, φ_i , we obtained a pair of best-fit coordinates (w_0, w_a) . Therefore, the set of initial field values defined a curve $w_a(w_0)$, which was approximately a line in most cases. Given this correspondence, the probability density function can be reduced to a single-variable function

$$p(w_0) \propto P(w_0, w_a(w_0)). \quad (17)$$

(Since most curves $w_a(w_0)$ are linear, this suffices for our analysis. To be precise, there is also a correction factor of the form $\sqrt{1 + w_a'(w_0)^2}$.) Since there is typically a maximum value for w_0 , $w_{0,\max}$, we will truncate $p(w_0)$ at that point, meaning that $p(w_0 > w_{0,\max}) = 0$. As described in [46], even if $w_0 = -1$ defines the left boundary of the domain, we extend the distribution to smaller values in order to assign a probability to the cosmological constant:

$$p_{\text{null}} = \frac{1}{\mathcal{N}} \int_{-\infty}^{-1} dw_0 p(w_0), \quad (18)$$

$$\mathcal{N} = \int_{-\infty}^{w_{0,\max}} dw_0 p(w_0). \quad (19)$$

Finally, one can translate this probability into a number of standard deviations as

$$N_\sigma = \sqrt{2} \operatorname{Erf}^{-1}(1 - 2p_{\text{null}}), \quad (20)$$

which is the usual way of quantifying the statistical tension.

The results are given in the tables at the end of the paper. We see that the number of standard deviations that the cosmological constant is in tension with the data is somewhat reduced compared to those reported by DESI in the entire w_0, w_a plane. An example is the cosine potential, which provides one of the better agreements between theory and observations. As can be seen in the table, for $k = 3$, we have the number of standard deviations as $N_\sigma \approx 1.5, 2.1, 3.1$, for Pantheon-Plus, Union3, and DESY5 data sets, respectively. This is somewhat worse than the standard deviations reported by DESI in the entire w_0, w_a plane of $N_\sigma = 2.8, 3.8, 4.2$, for each data set, respectively.

Although the tensions remain moderate in these models, we should also bear in mind that this involves new parameters, so there should be an additional penalty. Altogether, the tension of a cosmological constant in these models is arguably not large enough to significantly favor them over the null hypothesis.

Also, the fact that none of the models gives values in the w_0, w_a plane that lies right through the data suggests that these simple quintessence constructions may not be quite right. This leads us to now go beyond the minimal coupling for a broader class of models.

IV. NON-MINIMAL COUPLING

In this section, we will consider scalar fields non-minimally coupled to gravity. The action is given by

$$S = \int d^4x \sqrt{-g} \left[\frac{M_p^2}{2} R - \frac{1}{2} g^{\mu\nu} \partial_\mu \varphi \partial_\nu \varphi - V(\varphi) - \frac{1}{2} \xi \varphi^2 R + \mathcal{L}_m \right], \quad (21)$$

where ξ is the non-minimal coupling parameter. The energy-momentum tensor of the scalar field reads

$$T_{\mu\nu} = \partial_\mu \varphi \partial_\nu \varphi - g_{\mu\nu} \left[\frac{1}{2} g^{\alpha\beta} \partial_\alpha \varphi \partial_\beta \varphi + V(\varphi) \right] + \xi (G_{\mu\nu} + g_{\mu\nu} \square - \nabla_\mu \nabla_\nu) \varphi^2, \quad (22)$$

where $G_{\mu\nu}$ is the Einstein tensor. For an FLRW background, one finds the following expressions for the energy density and the pressure:

$$\rho_\varphi = \frac{1}{2} \dot{\varphi}^2 + V(\varphi) + 3H\xi (H\varphi^2 + 2\varphi\dot{\varphi}), \quad (23)$$

$$p_\varphi = \frac{1}{2} \dot{\varphi}^2 - V(\varphi) + \xi \left\{ -2\dot{\varphi}^2 + 2\varphi V'(\varphi) + \left[H^2 + 2 \left(\xi - \frac{1}{6} \right) R \right] \varphi^2 + 2H\varphi\dot{\varphi} \right\}. \quad (24)$$

Note that a non-vanishing coupling parameter allows, in principle, for NEC violation ($p_\varphi + \rho_\varphi < 0$). Therefore, if the value of ξ , the scalar potential and the initial conditions are appropriate, the dark energy equation of state can cross the phantom divide $w_\varphi = -1$ from below and provide a good fit to the DESI data [18, 19].

The evolution of the scalar field is found by numerically solving the equation of motion

$$\ddot{\varphi} + 3H\dot{\varphi} + V'(\varphi) + \xi R\varphi = 0, \quad (25)$$

with the Ricci scalar

$$R = \frac{\rho_m + \rho_\varphi - 3p_\varphi}{M_p^2}. \quad (26)$$

Also, we have the Friedmann equation (4).

As in section II, the initial value of the scalar field, φ_i , is chosen freely, and the initial velocity, $\dot{\varphi}_i$, is zero. The initial matter energy density is chosen to be much higher than the initial dark energy density; we pick the value 10^6 in our numerics. In order to do this, we first find the initial Hubble rate H_i as a function of the initial matter density $\rho_{m,i}$. Using Eqs. (4) and (23), one can show that

$$H_i = \frac{\xi\varphi_i\dot{\varphi}_i + \sqrt{\xi^2\varphi_i^2\dot{\varphi}_i^2 + \frac{1}{3}(M_p^2 - \xi\varphi_i^2)(\frac{1}{2}\dot{\varphi}_i^2 + V(\varphi_i) + \rho_{m,i})}}{M_p^2 - \xi\varphi_i^2}. \quad (27)$$

Then we substitute this into (23), set $\rho_{\varphi,i} = 10^{-6}\rho_{m,i}$ and solve for $\rho_{m,i}$. We note that in order for this form of dark energy to be very subdominant in the early universe can require significant fine-tuning of the initial conditions.

A. Fifth Force Constraints

The evolution of light, non-minimally coupled scalar fields is severely constrained by different tests of gravity.

Firstly, the presence of a light scalar leads to a new fifth force in the Solar System. To derive this, let us expand around the homogeneous field φ_0 today as

$$\varphi = \varphi_0 + \delta\varphi. \quad (28)$$

Then there is a linear term in the Lagrangian of the form

$$\Delta\mathcal{L} = -\xi\varphi_0\delta\varphi R = \left(\frac{\xi\varphi_0}{M_p^2}\right)\delta\varphi T, \quad (29)$$

where in the second step we have used the trace of the Einstein equations for matter $R = -T/M_p^2$ (so this is only valid on the equations of motion). This linear term means that fluctuations in the scalar are coupled to matter via an effective coupling $g = \xi\varphi_0/M_p^2$. This scalar $\delta\varphi$ mediates a fifth force between non-relativistic matter, but does not couple to light. In the weak field regime, we can express its consequences via the post-parameterized Newtonian parameter γ which is defined via the weak field metric Lagrangian $ds^2 = -(1 + 2\phi_N)dt^2 + (1 + 2\gamma\phi_N)|d\mathbf{x}|^2$. This leads to

$$\gamma = \frac{1 - 2g^2M_p^2}{1 + 2g^2M_p^2}. \quad (30)$$

The leading bound on γ comes from measurements of the Shapiro time delay of radio signals from the Cassini probe of $|\gamma - 1| < 2.3 \times 10^{-5}$. Inserting the above value for g , this leads to the following bound

$$\frac{|\xi\varphi_0|}{2.4 \times 10^{-3}M_p} < 1. \quad (31)$$

We will refer to this bound as the “Solar System constraint”. Defining

$$s(t) = \frac{\xi\varphi(t)}{2.4 \times 10^{-3}M_p}, \quad (32)$$

the constraint reads $|s_0| < 1$.

B. Gravitational Coupling Constraints

Secondly, as one can easily check from the action (21), the strength of gravity is controlled by an effective gravitational constant which depends on time⁵:

$$G_{\text{eff}} = \frac{G}{1 - \xi \left(\frac{\varphi}{M_p} \right)^2}. \quad (33)$$

The time variation of this function is bounded [51–53]:

$$\left| \frac{\dot{G}_{\text{eff}}}{G_{\text{eff}}} \right|_0 \lesssim 10^{-12} \text{ yr}^{-1}. \quad (34)$$

Taking the time derivative of (33), we get

$$\left| \frac{\dot{G}_{\text{eff}}}{G_{\text{eff}}} \right|_0 = \left| \frac{2\xi\varphi\dot{\varphi}}{M_p^2 - \xi\varphi^2} \right|_0 \lesssim 10^{-12} \text{ yr}^{-1}. \quad (35)$$

We will refer to this bound as the “effective gravitational constant constraint”.

The recent study [20] suggests that the values of ξ and φ today (φ_0) that are required to explain the DESI data are inconsistent with these bounds, implying that the theory (21) would have to be supplemented with extra ingredients. However, in what follows, we present an example (albeit fine-tuned) that seems to comply with the above constraints.

C. Choice of Frame

A subtlety is the choice of frame that we use to compare the predictions of our theory to the DESI data. As it stands, the action (21) is written in the so-called Jordan frame. In this frame, the matter fields are minimally coupled to the Jordan metric. By means of a Weyl transformation of the metric and a field redefinition, one could rewrite the theory in the Einstein frame and get an action which looks like the standard action for a scalar field minimally coupled to gravity. However, the couplings of the matter fields to the new

⁵ In [47–50], similar models with early time variation of the gravitational constant have been analyzed and tested against observations with a focus on their potential to alleviate the Hubble tension.

metric (the Einstein metric) are now φ -dependent; which manifests as a fifth force. Some discussion on the relation between the frames includes Refs. [54, 55].

An important related question is which of the frames is appropriate to directly test the theory against observations. While both frames are valid (since they are just related by field redefinitions), the Jordan frame seems to be more convenient for a direct comparison. The matter fields move on geodesics of the Jordan metric in the Jordan frame, but matter fields do not move on geodesics of the Einstein metric in the Einstein frame due to the additional fifth force. An implicit assumption behind the derivation of the usual distance-redshift and magnitude-redshift relations is that matter follows geodesics of the FLRW metric. The redshift is defined as $z = -1 + \lambda_0/\lambda_e$, where λ_0 is the wavelength of the light from a distant source we observe today and λ_e is supposed to be the wavelength of the light when it was emitted by the source. The value of λ_e is actually determined from the light emitted by atoms in an experiment on Earth, and we assume this is the wavelength with which light was emitted by the distant source in the past. However, this interpretation would not be correct in general in the Einstein frame, because atomic transition frequencies in this frame are φ -dependent due to the non-minimal coupling of the matter fields to the metric. Therefore, in order to compare the predictions of the Einstein-frame action to observations, one would have to take this fact into account. Ref. [56] provides more details.

D. Results

Here we present an example that satisfies the above fifth force restrictions. Moreover, its CPL parameters w_0, w_a will lie inside of one or more of the 2σ DESI contours. We considered the simple linear potential

$$V(\varphi) = V_0 \left(1 + \frac{k\varphi}{M_p} \right). \quad (36)$$

In this model, k acts as a parameter, in addition to the initial condition φ_i . However, to illustrate the basic idea, we will focus here on the following values:

$$k = 1, \quad \varphi_i = 0.08M_p. \quad (37)$$

In Fig. 6, we display the CPL parameters in the w_0, w_a plane for several values of the non-minimal coupling ξ . Also shown is the Solar System constraint (31), which is only satisfied for a small range of ξ values around $\xi \approx -0.5$. A zoom in on this region is also shown in the figure.

The value of the field φ as a function of time, as well as the matter and dark energy density fractions and the equation of state, are shown in Fig. 7 for the particular case $\xi = -0.506$. The constraints in this case are plotted in Fig. 8. In order to directly test the gravitational

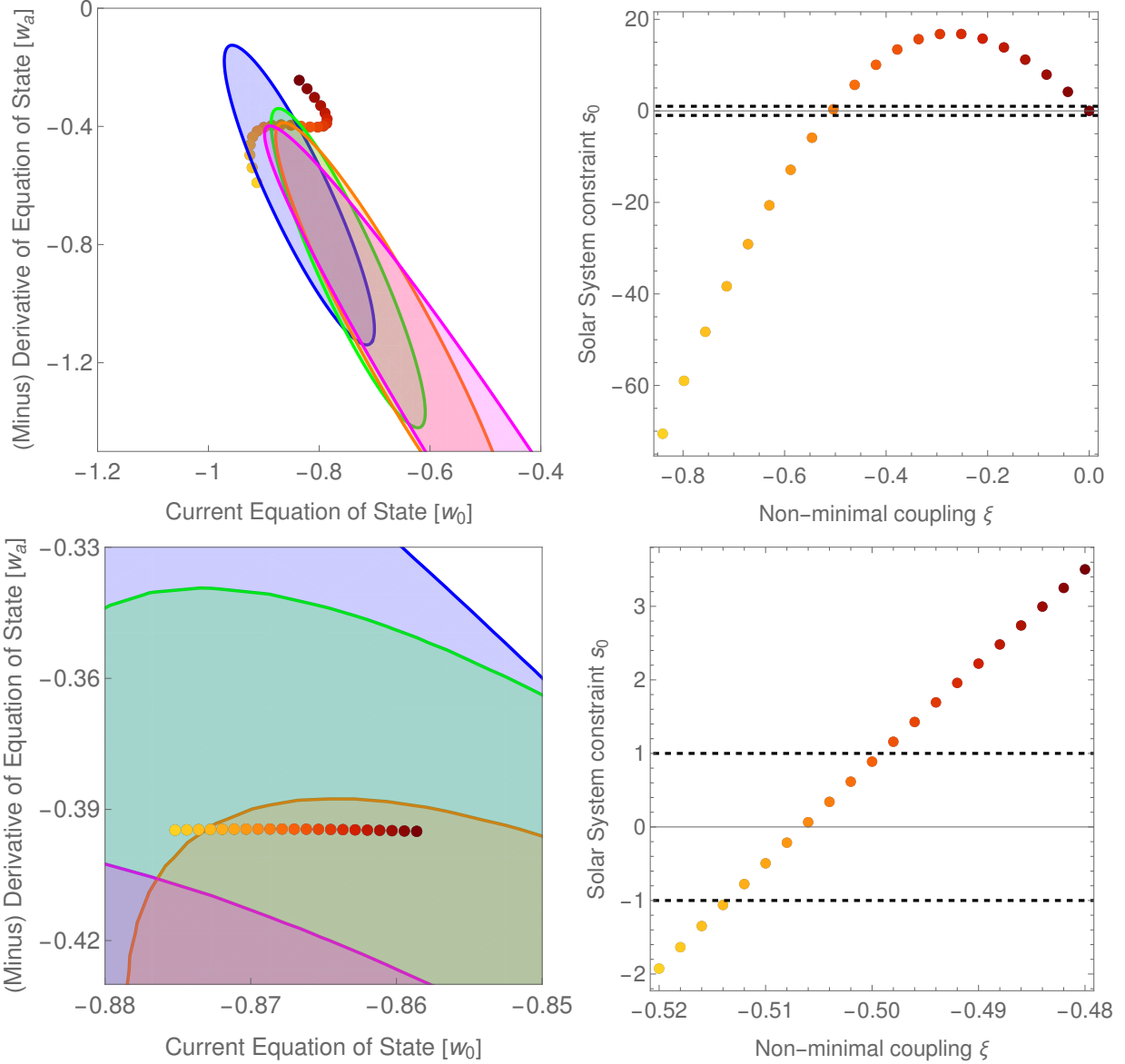


FIG. 6. Top left: DESI 2σ contours and (w_0, w_a) points for the values of non-minimal couplings ξ indicated on the right. Top right: Solar System constraint (31) for different values of ξ . The dashed lines indicate the lower and upper bounds (-1 and 1). Bottom panels are a zoomed in version focusing on $-0.52 < \xi < -0.48$. These plots are for $k = 1$, $\varphi_i = 0.08M_p$.

constant constraint (35), we must adapt it to our units. We are measuring time in units of m^{-1} ; let us call this dimensionless time $\tilde{t} \equiv m t$. Solving the equations numerically, we can output a dimensionless Hubble parameter today as

$$\tilde{H}_0 = \frac{1}{a} \frac{da}{d\tilde{t}} \Big|_0 \quad (38)$$

where the physical Hubble parameter is $H_0 = \tilde{H}_0 m$. For the specific case $\xi = -0.506$, we

find $\tilde{H}_0 \approx 0.71$. Using the measured value of Hubble parameter $H_0 \approx 6.91 \times 10^{-11} \text{ yr}^{-1}$ [57], we get $m \approx 9.73 \times 10^{-11} \text{ yr}^{-1}$, so the dimensionless right-hand-side of (34) and (35) is $10^{-12} \text{ yr}^{-1}/m \approx 0.0103$. This is the bound indicated in the right panel of Fig. 8. Finally, the time evolution of G_{eff}/G is shown in Fig. 9.

We have carefully chosen parameters (fine-tuned) that satisfy the current solar system and time evolution bounds today. For the solar system bound, this is because φ is “accidentally” small today, though it was large in both the past and the future in these models, as seen in Fig. 7. As far as we are aware, this is consistent with observations. For the $\dot{G}_{\text{eff}}/G_{\text{eff}}$ bound, we note that it is slightly outside the current bound (10^{-12} yr^{-1}) in the past. Whether this is in tension with observations is not clear to us.

Finally, we note that in our construction, nothing prevents the scalar field from dominating the energy density of the universe at redshifts higher than the one corresponding to our initial condition. The shape of the potential and the coupling to the Ricci scalar chosen in this example need to be modified to some extent in order for dark energy to be subdominant at early times, including recombination, matter-radiation equality and earlier.

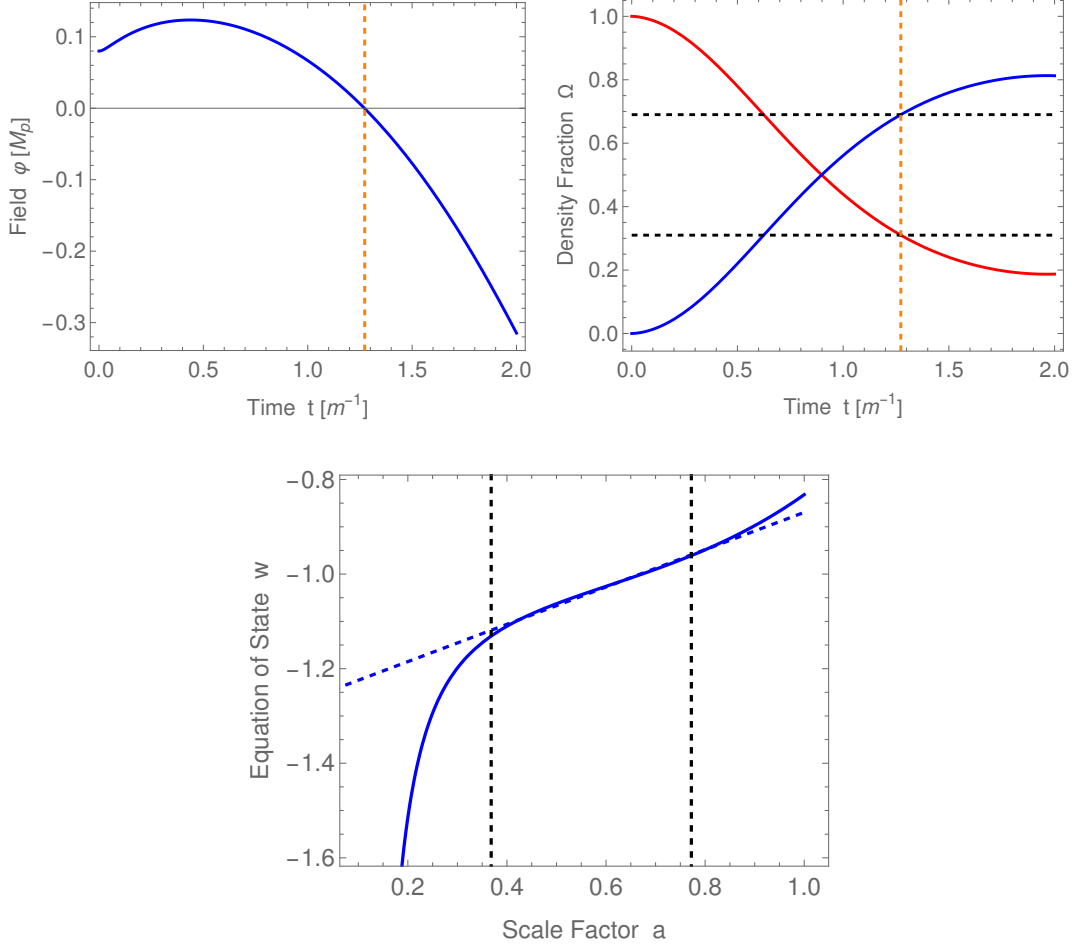


FIG. 7. Top left: Value of the scalar field as a function of time. Top right: Fractional energy densities of matter (red) and dark energy (blue). The vertical dashed line (orange) corresponds to the current time, defined as the moment at which the dark energy density fraction becomes $\Omega_{DE,0} = 0.69$, which in this case is $t_0 \approx 1.27m^{-1}$. Bottom: Dark energy equation of state w as a function of the scale factor (solid curve) and CPL fit (blue dashed line). The vertical lines indicate the range over which DESI is most sensitive. The present time is at $a = 1$. These plots are for the non-minimally coupled model with $k = 1$, $\varphi_i = 0.08M_p$, $\xi = -0.506$.

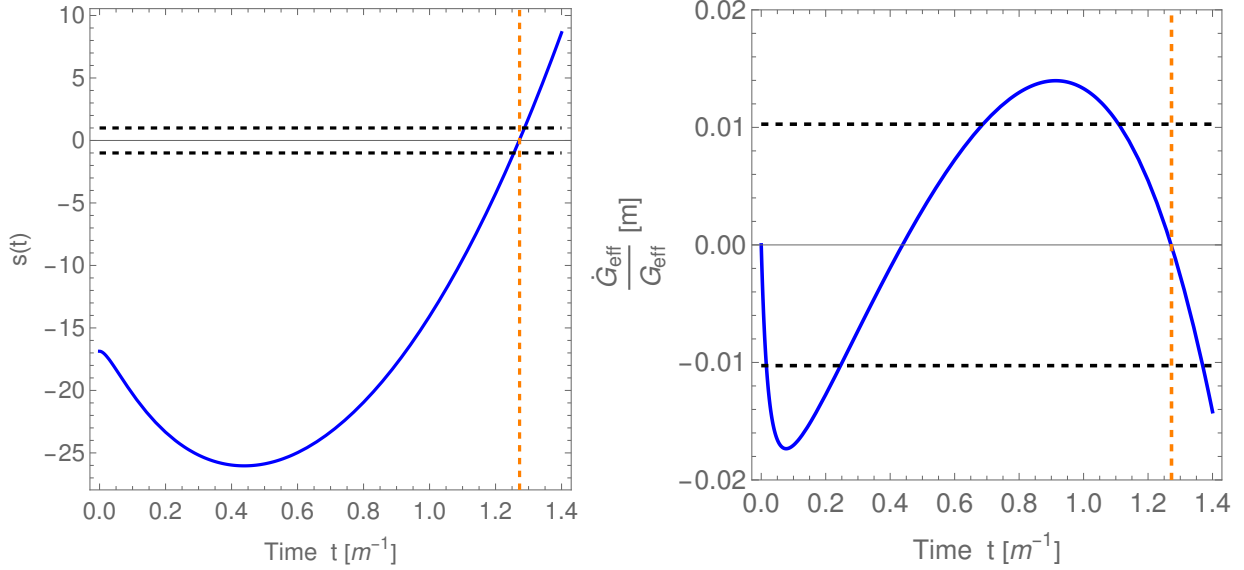


FIG. 8. Solar System (left) and effective gravitational constant (right) constraints versus time. The vertical dashed line (orange) corresponds to the current time $t_0 \approx 1.27m^{-1}$, and the horizontal dashed lines indicate the lower and upper bounds today. This is for the non-minimally coupled model with $k = 1$, $\varphi_i = 0.08M_p$, $\xi = -0.506$.

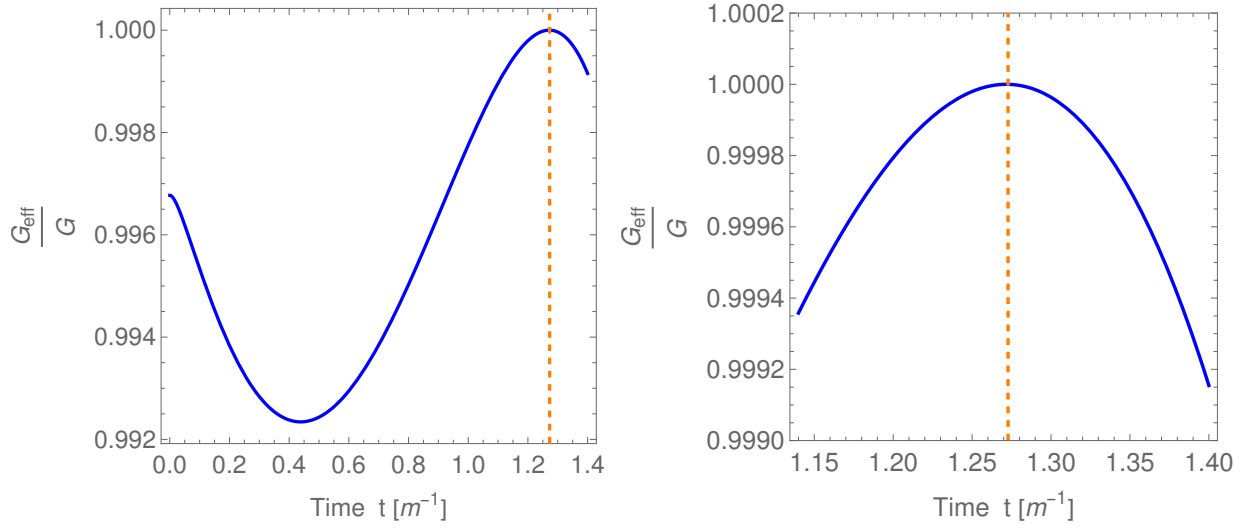


FIG. 9. Time evolution of the effective gravitational constant. The vertical dotted line corresponds to the current time $t_0 \approx 1.27m^{-1}$. The panel on the right is a zoomed-in view near the current time.

V. DISCUSSION

In this work, we have explored a large range of quintessence models in light of the 2025 DESI data on dark energy. For minimally coupled scalar fields, we have found that the statistical significance is reduced compared to that reported by the DESI analysis in the entire w_0, w_a plane (with equation of state of dynamical dark energy $w = w_0 + (1 - a)w_a$). While some models show reasonable agreement, none are able to reach inside the 2σ region of the data.

For non-minimally scalar fields, one can arrange for an improved fit to the data. However, this implies a new fifth force and a dynamical value for the effective Newton's gravitational coupling G . Both are tightly constrained by tests of gravity. For some carefully selected values, we can escape bounds from the Solar System by having the fifth force "accidentally" be suppressed today. The bound on the evolution of Newton's coupling is able to be obeyed today, though there are moments in the history of the universe where our existing example is outside the bounds; see right panel in Fig. 8. Whether this is in tension with other bounds is less clear. From Fig. 9 this implies a shifted value of G in the very early universe, including Big Bang Nucleosynthesis. However, in this example, the shift is only at the level $\sim 0.3\%$ (we have not directly included radiation in our analysis to be certain, and as mentioned earlier, some modification of the theory is required to properly handle the very early universe). It would be interesting to provide further constraints on these kinds of model in the future.

Overall, generic models of quintessence can provide moderate improvement in fitting the DESI data compared to a cosmological constant. However, the presence of additional parameters means that there should be a penalty in such models. For very narrow ranges of non-minimally coupled models (fine-tuned) one can provide significant improvement in fitting the data, as well as evading some basic tests of gravity. Further work can involve a more systematic exploration of the full parameter space.

VI. ACKNOWLEDGMENTS

M. P.-H. is supported in part by National Science Foundation grants PHY-2310572 and PHY-2419848. D. J.-A. is supported in part by National Science Foundation grant PHY-2419848. We thank the VERSE program at Tufts for support. We thank David Kaiser for discussion.

[1] A. G. Riess *et al.* (Supernova Search Team), Observational evidence from supernovae for an accelerating universe and a cosmological constant, *Astron. J.* **116**, 1009 (1998), [arXiv:astro-ph/9805201](https://arxiv.org/abs/astro-ph/9805201).

[2] S. Perlmutter *et al.* (Supernova Cosmology Project), Measurements of Ω and Λ from 42 High Redshift Supernovae, *Astrophys. J.* **517**, 565 (1999), [arXiv:astro-ph/9812133](https://arxiv.org/abs/astro-ph/9812133).

[3] S. Weinberg, The cosmological constant problem, *Rev. Mod. Phys.* **61**, 1 (1989).

[4] A. G. Adame *et al.* (DESI), DESI 2024 VI: cosmological constraints from the measurements of baryon acoustic oscillations, *JCAP* **02**, 021, [arXiv:2404.03002 \[astro-ph.CO\]](https://arxiv.org/abs/2404.03002).

[5] M. Abdul Karim *et al.* (DESI), DESI DR2 Results II: Measurements of Baryon Acoustic Oscillations and Cosmological Constraints, (2025), [arXiv:2503.14738 \[astro-ph.CO\]](https://arxiv.org/abs/2503.14738).

[6] M. Chevallier and D. Polarski, Accelerating universes with scaling dark matter, *Int. J. Mod. Phys. D* **10**, 213 (2001), [arXiv:gr-qc/0009008](https://arxiv.org/abs/gr-qc/0009008).

[7] E. V. Linder, Exploring the expansion history of the universe, *Phys. Rev. Lett.* **90**, 091301 (2003), [arXiv:astro-ph/0208512](https://arxiv.org/abs/astro-ph/0208512).

[8] S. Dutta and R. J. Scherrer, Hilltop Quintessence, *Phys. Rev. D* **78**, 123525 (2008), [arXiv:0809.4441 \[astro-ph\]](https://arxiv.org/abs/0809.4441).

[9] T. Chiba, Slow-Roll Thawing Quintessence, *Phys. Rev. D* **79**, 083517 (2009), [Erratum: *Phys. Rev. D* 80, 109902 (2009)], [arXiv:0902.4037 \[astro-ph.CO\]](https://arxiv.org/abs/0902.4037).

[10] S. Bhattacharya, G. Borghetto, A. Malhotra, S. Parameswaran, G. Tasinato, and I. Zavala, Cosmological constraints on curved quintessence, *JCAP* **09**, 073, [arXiv:2405.17396 \[astro-ph.CO\]](https://arxiv.org/abs/2405.17396).

[11] S. Bhattacharya, G. Borghetto, A. Malhotra, S. Parameswaran, G. Tasinato, and I. Zavala, Cosmological tests of quintessence in quantum gravity, *JCAP* **04**, 086, [arXiv:2410.21243 \[astro-ph.CO\]](https://arxiv.org/abs/2410.21243).

[12] S. Nesseris, Y. Akrami, and G. D. Starkman, To CPL, or not to CPL? What we have not learned about the dark energy equation of state, (2025), [arXiv:2503.22529 \[astro-ph.CO\]](https://arxiv.org/abs/2503.22529).

[13] B. R. Dinda and R. Maartens, Physical vs phantom dark energy after DESI: thawing quintessence in a curved background, *Mon. Not. Roy. Astron. Soc.* **542**, L31 (2025), [arXiv:2504.15190 \[astro-ph.CO\]](https://arxiv.org/abs/2504.15190).

[14] E. Özülker, E. Di Valentino, and W. Giarè, Dark Energy Crosses the Line: Quantifying and Testing the Evidence for Phantom Crossing, (2025), [arXiv:2506.19053 \[astro-ph.CO\]](https://arxiv.org/abs/2506.19053).

[15] I. D. Gialamas, G. Hütsi, M. Raidal, J. Urrutia, M. Vasar, and H. Veermäe, Quintessence and phantoms in light of DESI 2025, (2025), [arXiv:2506.21542 \[astro-ph.CO\]](https://arxiv.org/abs/2506.21542).

- [16] S. Roy Choudhury and T. Okumura, Updated Cosmological Constraints in Extended Parameter Space with Planck PR4, DESI Baryon Acoustic Oscillations, and Supernovae: Dynamical Dark Energy, Neutrino Masses, Lensing Anomaly, and the Hubble Tension, *Astrophys. J. Lett.* **976**, L11 (2024), arXiv:2409.13022 [astro-ph.CO].
- [17] S. Roy Choudhury, Cosmology in Extended Parameter Space with DESI Data Release 2 Baryon Acoustic Oscillations: A $2\sigma+$ Detection of Nonzero Neutrino Masses with an Update on Dynamical Dark Energy and Lensing Anomaly, *Astrophys. J. Lett.* **986**, L31 (2025), arXiv:2504.15340 [astro-ph.CO].
- [18] G. Ye, M. Martinelli, B. Hu, and A. Silvestri, Hints of Nonminimally Coupled Gravity in DESI 2024 Baryon Acoustic Oscillation Measurements, *Phys. Rev. Lett.* **134**, 181002 (2025), arXiv:2407.15832 [astro-ph.CO].
- [19] W. J. Wolf, P. G. Ferreira, and C. García-García, Matching current observational constraints with nonminimally coupled dark energy, *Phys. Rev. D* **111**, L041303 (2025), arXiv:2409.17019 [astro-ph.CO].
- [20] W. J. Wolf, C. García-García, T. Anton, and P. G. Ferreira, Assessing Cosmological Evidence for Nonminimal Coupling, *Phys. Rev. Lett.* **135**, 081001 (2025), arXiv:2504.07679 [astro-ph.CO].
- [21] J.-Q. Wang, R.-G. Cai, Z.-K. Guo, and S.-J. Wang, Resolving the Planck-DESI tension by non-minimally coupled quintessence, (2025), arXiv:2508.01759 [astro-ph.CO].
- [22] A. Giacomini, G. Leon, A. Paliathanasis, and S. Pan, Cosmological Evolution of Two-Scalar fields Cosmology in the Jordan frame, *Eur. Phys. J. C* **80**, 184 (2020), arXiv:2001.02414 [gr-qc].
- [23] D. Andriot, Phantom matters, *Phys. Dark Univ.* **49**, 102000 (2025), arXiv:2505.10410 [hep-th].
- [24] S. S. Mishra, W. L. Matthewson, V. Sahni, A. Shafieloo, and Y. Shtanov, Braneworld Dark Energy in light of DESI DR2, (2025), arXiv:2507.07193 [astro-ph.CO].
- [25] T.-N. Li, P.-J. Wu, G.-H. Du, S.-J. Jin, H.-L. Li, J.-F. Zhang, and X. Zhang, Constraints on Interacting Dark Energy Models from the DESI Baryon Acoustic Oscillation and DES Supernovae Data, *Astrophys. J.* **976**, 1 (2024), arXiv:2407.14934 [astro-ph.CO].
- [26] T.-N. Li, G.-H. Du, Y.-H. Li, P.-J. Wu, S.-J. Jin, J.-F. Zhang, and X. Zhang, Probing the sign-changeable interaction between dark energy and dark matter with DESI baryon acoustic oscillations and DES supernovae data, (2025), arXiv:2501.07361 [astro-ph.CO].
- [27] A. Chakraborty, P. K. Chanda, S. Das, and K. Dutta, DESI results: Hint towards coupled dark matter and dark energy, (2025), arXiv:2503.10806 [astro-ph.CO].
- [28] M. van der Westhuizen, D. Figueruelo, R. Thubisi, S. Sahlu, A. Abebe, and A. Paliathanasis, Compartmentalization in the Dark Sector of the Universe after DESI DR2 BAO data, (2025), arXiv:2505.23306 [astro-ph.CO].

[29] S. L. Guedezounme, B. R. Dinda, and R. Maartens, Phantom crossing or dark interaction?, (2025), [arXiv:2507.18274 \[astro-ph.CO\]](https://arxiv.org/abs/2507.18274).

[30] A. A. Samanta, A. Ajith, and S. Panda, Exploring Coupled Quintessence in light of CMB and DESI DR2 measurements, (2025), [arXiv:2509.09624 \[gr-qc\]](https://arxiv.org/abs/2509.09624).

[31] B. Wang, E. Abdalla, F. Atrio-Barandela, and D. Pavón, Further understanding the interaction between dark energy and dark matter: current status and future directions, *Rept. Prog. Phys.* **87**, 036901 (2024), [arXiv:2402.00819 \[astro-ph.CO\]](https://arxiv.org/abs/2402.00819).

[32] S. Goldstein, M. Celoria, and F. Schmidt, Monodromic Dark Energy and DESI, (2025), [arXiv:2507.16970 \[astro-ph.CO\]](https://arxiv.org/abs/2507.16970).

[33] R. Chen, J. M. Cline, V. Muralidharan, and B. Salewicz, Quintessential dark energy crossing the phantom divide, (2025), [arXiv:2508.19101 \[astro-ph.CO\]](https://arxiv.org/abs/2508.19101).

[34] N. Dimakis, K. J. Duffy, A. Giacomini, A. Y. Kamenshchik, G. Leon, and A. Paliathanasis, Mapping solutions in nonmetricity gravity: Investigating cosmological dynamics in conformal equivalent theories, *Phys. Dark Univ.* **44**, 101436 (2024), [arXiv:2312.11208 \[gr-qc\]](https://arxiv.org/abs/2312.11208).

[35] Y. Yang, Q. Wang, X. Ren, E. N. Saridakis, and Y.-F. Cai, Modified Gravity Realizations of Quintom Dark Energy after DESI DR2, *Astrophys. J.* **988**, 123 (2025), [arXiv:2504.06784 \[astro-ph.CO\]](https://arxiv.org/abs/2504.06784).

[36] A. Paliathanasis, Testing non-coincident $f(Q)$ -gravity with DESI DR2 BAO and GRBs, *Phys. Dark Univ.* **49**, 101993 (2025), [arXiv:2504.11132 \[gr-qc\]](https://arxiv.org/abs/2504.11132).

[37] A. Paliathanasis, Observational Constraints on Scalar Field–Matter Interaction in Weyl Integrable Spacetime, (2025), [arXiv:2506.16223 \[gr-qc\]](https://arxiv.org/abs/2506.16223).

[38] S. Nojiri, S. D. Odintsov, and V. K. Oikonomou, Phantom Crossing and Oscillating Dark Energy with $F(R)$ Gravity, (2025), [arXiv:2506.21010 \[gr-qc\]](https://arxiv.org/abs/2506.21010).

[39] M. Höglås and E. Mörtsell, Bimetric gravity improves the fit to DESI BAO and eases the Hubble tension, (2025), [arXiv:2507.03743 \[astro-ph.CO\]](https://arxiv.org/abs/2507.03743).

[40] U. Kumar, A. Ajith, and A. Verma, Evidence for non-cold dark matter from DESI DR2 measurements, (2025), [arXiv:2504.14419 \[astro-ph.CO\]](https://arxiv.org/abs/2504.14419).

[41] X. Chen and A. Loeb, Evolving dark energy or dark matter with an evolving equation-of-state?, *JCAP* **07**, 059, [arXiv:2505.02645 \[astro-ph.CO\]](https://arxiv.org/abs/2505.02645).

[42] M. Braglia, X. Chen, and A. Loeb, Exotic Dark Matter and the DESI Anomaly, (2025), [arXiv:2507.13925 \[astro-ph.CO\]](https://arxiv.org/abs/2507.13925).

[43] G. G. Luciano, A. Paliathanasis, and E. N. Saridakis, Barrow and Tsallis entropies after the DESI DR2 BAO data, *JCAP* **09**, 013, [arXiv:2504.12205 \[gr-qc\]](https://arxiv.org/abs/2504.12205).

[44] A. Paliathanasis, Dark energy within the generalized uncertainty principle in light of DESI DR2, *JCAP* **09**, 067, [arXiv:2503.20896 \[astro-ph.CO\]](https://arxiv.org/abs/2503.20896).

[45] M. Scherer, M. A. Sabogal, R. C. Nunes, and A. De Felice, Challenging the Λ CDM model: 5σ evidence for a dynamical dark energy late-time transition, *Phys. Rev. D* **112**, 043513 (2025), arXiv:2504.20664 [astro-ph.CO].

[46] Z. Bayat and M. P. Hertzberg, Examining quintessence models with DESI data, *JCAP* **08**, 065, arXiv:2505.18937 [astro-ph.CO].

[47] M. Rossi, M. Ballardini, M. Braglia, F. Finelli, D. Paoletti, A. A. Starobinsky, and C. Umiltà, Cosmological constraints on post-Newtonian parameters in effectively massless scalar-tensor theories of gravity, *Phys. Rev. D* **100**, 103524 (2019), arXiv:1906.10218 [astro-ph.CO].

[48] M. Braglia, M. Ballardini, W. T. Emond, F. Finelli, A. E. Gumrukcuoglu, K. Koyama, and D. Paoletti, Larger value for H_0 by an evolving gravitational constant, *Phys. Rev. D* **102**, 023529 (2020), arXiv:2004.11161 [astro-ph.CO].

[49] M. Braglia, M. Ballardini, F. Finelli, and K. Koyama, Early modified gravity in light of the H_0 tension and LSS data, *Phys. Rev. D* **103**, 043528 (2021), arXiv:2011.12934 [astro-ph.CO].

[50] G. Franco Abellán, M. Braglia, M. Ballardini, F. Finelli, and V. Poulin, Probing early modification of gravity with Planck, ACT and SPT, *JCAP* **12**, 017, arXiv:2308.12345 [astro-ph.CO].

[51] T. Damour and K. Nordtvedt, General relativity as a cosmological attractor of tensor scalar theories, *Phys. Rev. Lett.* **70**, 2217 (1993).

[52] T. Damour and K. Nordtvedt, Tensor - scalar cosmological models and their relaxation toward general relativity, *Phys. Rev. D* **48**, 3436 (1993).

[53] J.-P. Uzan, Fundamental constants: from measurement to the universe, a window on gravitation and cosmology, (2024), arXiv:2410.07281 [astro-ph.CO].

[54] V. Faraoni, *Cosmology in scalar tensor gravity* (2004).

[55] V. Faraoni and S. Capozziello, *Beyond Einstein Gravity: A Survey of Gravitational Theories for Cosmology and Astrophysics* (Springer, Dordrecht, 2011).

[56] T. Chiba and M. Yamaguchi, Conformal-Frame (In)dependence of Cosmological Observations in Scalar-Tensor Theory, *JCAP* **10**, 040, arXiv:1308.1142 [gr-qc].

[57] Y. Akrami *et al.* (Planck), Planck 2018 results. X. Constraints on inflation, *Astron. Astrophys.* **641**, A10 (2020), arXiv:1807.06211 [astro-ph.CO].

Model: $V(\varphi) = V_0 \left(1 - \frac{k^2}{2M_p^2} \varphi^2\right)$									
	Pan-Plus		Union3		DESY5		CMB		
	p_{null}	N_{σ}	p_{null}	N_{σ}	p_{null}	N_{σ}	p_{null}	N_{σ}	
$k=1$	0.088	1.352	0.030	1.882	0.002	2.920	0.471	0.072	
$k=1.2$	0.086	1.366	0.029	1.902	0.002	2.936	0.464	0.089	
$k=1.4$	0.083	1.383	0.027	1.925	0.002	2.954	0.457	0.109	
$k=1.6$	0.081	1.400	0.026	1.949	0.001	2.973	0.448	0.130	
$k=1.8$	0.078	1.418	0.024	1.973	0.001	2.993	0.440	0.151	
$k=2$	0.075	1.437	0.023	1.994	0.001	3.013	0.433	0.169	
$k=2.5$	0.069	1.483	0.022	2.005	0.001	3.049	0.424	0.191	
$k=3$	0.066	1.510	0.029	1.893	0.001	2.977	0.443	0.144	
$k=4$	0.099	1.287	0.089	1.350	0.009	2.366	0.560	-	
$k=5$	0.250	0.675	0.274	0.600	0.076	1.429	0.729	-	
$k=6$	0.453	0.118	0.493	0.017	0.243	0.697	0.841	-	
$k=7$	0.672	-	0.708	-	0.500	0.001	0.894	-	
$k=8$	0.819	-	0.841	-	0.715	-	0.926	-	
$k=9$	0.640	-	0.668	-	0.636	-	0.689	-	
$k=10$	0.871	-	0.884	-	0.881	-	0.885	-	

Model: $V(\varphi) = V_0 \left(1 - \frac{k^4}{4M_p^4} \varphi^4\right)$									
	Pan-Plus		Union3		DESY5		CMB		
	p_{null}	N_{σ}	p_{null}	N_{σ}	p_{null}	N_{σ}	p_{null}	N_{σ}	
$k=0.5$	0.082	1.390	0.027	1.920	0.002	2.952	0.457	0.107	
$k=1$	0.076	1.433	0.024	1.972	0.001	2.998	0.439	0.153	
$k=1.6$	0.071	1.469	0.028	1.913	0.001	2.987	0.447	0.133	
$k=2$	0.072	1.464	0.036	1.794	0.002	2.884	0.470	0.074	
$k=4$	0.181	0.911	0.191	0.875	0.037	1.782	0.672	-	
$k=8$	0.602	-	0.637	-	0.401	0.251	0.897	-	

Model: $V(\varphi) = V_0 \left(1 - \frac{k^2}{2M_p^2} \varphi^2 + \frac{\lambda k^4}{16M_p^4} \varphi^4\right)$							
	Pan-Plus		Union3		DESY5		CMB
	p_{null}	N_{σ}	p_{null}	N_{σ}	p_{null}	N_{σ}	p_{null}
$k=1, \lambda = 0.32$	0.089	1.348	0.030	1.875	0.002	2.914	0.474 0.065
$k=1.5, \lambda = 0.32$	0.083	1.388	0.027	1.930	0.002	2.958	0.455 0.114
$k=2, \lambda = 0.32$	0.076	1.434	0.023	1.993	0.001	3.009	0.433 0.169
$k=1, \lambda = 0.48$	0.089	1.347	0.031	1.871	0.002	2.911	0.475 0.062
$k=1.5, \lambda = 0.48$	0.083	1.387	0.027	1.927	0.002	2.956	0.456 0.111
$k=2, \lambda = 0.48$	0.076	1.433	0.023	1.991	0.001	3.006	0.433 0.168
$k=1, \lambda = 0.64$	0.089	1.345	0.031	1.867	0.002	2.908	0.477 0.058
$k=1.5, \lambda = 0.64$	0.083	1.385	0.027	1.923	0.002	2.953	0.457 0.108
$k=2, \lambda = 0.64$	0.076	1.432	0.023	1.988	0.001	3.004	0.434 0.166
$k=1, \lambda = 0.8$	0.090	1.343	0.031	1.862	0.002	2.904	0.478 0.054
$k=1.5, \lambda = 0.8$	0.083	1.383	0.028	1.919	0.002	2.950	0.458 0.104
$k=2, \lambda = 0.8$	0.076	1.430	0.024	1.985	0.001	3.002	0.435 0.164
$k=1, \lambda = 0.96$	0.090	1.340	0.032	1.857	0.002	2.900	0.480 0.050
$k=1.5, \lambda = 0.96$	0.084	1.382	0.028	1.914	0.002	2.947	0.460 0.101
$k=2, \lambda = 0.96$	0.077	1.429	0.024	1.981	0.001	2.999	0.436 0.162

Model: $V(\varphi) = V_0 \left(1 - \frac{k^2}{2M_p^2} \varphi^2 + \frac{k^4}{16M_p^4} \varphi^4 \right)$									
	Pan-Plus		Union3		DESY5		CMB		
	p_{null}	N_{σ}	p_{null}	N_{σ}	p_{null}	N_{σ}	p_{null}	N_{σ}	
$k=0.5$	0.095	1.310	0.035	1.813	0.002	2.865	0.494	0.015	
$k=1$	0.090	1.340	0.032	1.855	0.002	2.899	0.480	0.049	
$k=1.2$	0.088	1.355	0.030	1.877	0.002	2.917	0.473	0.068	
$k=1.4$	0.085	1.372	0.029	1.901	0.002	2.936	0.465	0.089	
$k=1.5$	0.084	1.381	0.028	1.913	0.002	2.946	0.460	0.100	
$k=1.6$	0.082	1.390	0.027	1.926	0.002	2.956	0.456	0.111	
$k=1.8$	0.079	1.409	0.025	1.953	0.001	2.977	0.446	0.136	
$k=2$	0.077	1.428	0.024	1.981	0.001	2.999	0.436	0.161	
$k=2.5$	0.070	1.476	0.020	2.047	0.001	3.052	0.412	0.222	
$k=3$	0.064	1.520	0.020	2.056	0.001	3.089	0.406	0.239	
$k=3.5$	0.061	1.546	0.026	1.942	0.001	3.021	0.426	0.187	
$k=4$	0.071	1.467	0.049	1.651	0.003	2.720	0.489	0.029	
$k=4.5$	0.102	1.270	0.094	1.316	0.010	2.321	0.565	-	
$k=5$	0.172	0.946	0.183	0.904	0.035	1.810	0.660	-	
$k=5.5$	0.260	0.645	0.286	0.566	0.083	1.384	0.735	-	
$k=6$	0.259	0.648	0.285	0.567	0.083	1.385	0.734	-	
$k=6.5$	0.511	-	0.552	-	0.304	0.514	0.863	-	
$k=7$	0.617	-	0.655	-	0.427	0.183	0.892	-	
$k=7.5$	0.715	-	0.746	-	0.555	-	0.928	-	
$k=8$	0.786	-	0.811	-	0.657	-	0.946	-	
$k=8.5$	0.847	-	0.858	-	0.748	-	0.946	-	
$k=9$	0.893	-	0.903	-	0.820	-	0.966	-	
$k=9.5$	0.927	-	0.935	-	0.877	-	0.978	-	
$k=10$	0.950	-	0.957	-	0.916	-	0.984	-	

Model: $V(\varphi) = \frac{V_0}{2} \left(1 + \cos\left(\frac{\sqrt{2}k\varphi}{M_p}\right)\right)$									
	Pan-Plus		Union3		DESY5		CMB		
	p_{null}	N_{σ}	p_{null}	N_{σ}	p_{null}	N_{σ}	p_{null}	N_{σ}	
$k=0.5$	0.096	1.307	0.035	1.806	0.002	2.859	0.497	0.007	
$k=1$	0.091	1.336	0.032	1.846	0.002	2.892	0.483	0.042	
$k=1.2$	0.088	1.351	0.031	1.868	0.002	2.910	0.476	0.060	
$k=1.4$	0.086	1.368	0.029	1.892	0.002	2.929	0.467	0.082	
$k=1.6$	0.083	1.387	0.028	1.918	0.002	2.950	0.458	0.105	
$k=1.8$	0.080	1.406	0.026	1.946	0.001	2.972	0.448	0.130	
$k=2$	0.077	1.426	0.024	1.974	0.001	2.994	0.438	0.155	
$k=2.5$	0.070	1.474	0.020	2.044	0.001	3.048	0.413	0.221	
$k=3$	0.064	1.519	0.017	2.109	0.001	3.097	0.388	0.286	
$k=3.5$	0.060	1.552	0.023	1.995	0.001	3.063	0.414	0.218	
$k=4$	0.067	1.498	0.043	1.719	0.003	2.795	0.473	0.068	
$k=4.5$	0.084	1.376	0.070	1.473	0.006	2.509	0.528	-	
$k=5$	0.134	1.107	0.136	1.096	0.020	2.049	0.616	-	
$k=5.5$	0.216	0.784	0.236	0.718	0.058	1.575	0.702	-	
$k=6$	0.348	0.391	0.383	0.298	0.148	1.047	0.789	-	
$k=6.5$	0.474	0.066	0.514	-	0.264	0.631	0.848	-	
$k=7$	0.599	-	0.638	-	0.406	0.238	0.894	-	
$k=7.5$	0.624	-	0.662	-	0.437	0.159	0.902	-	
$k=8$	0.716	-	0.748	-	0.558	-	0.930	-	
$k=8.5$	0.829	-	0.850	-	0.722	-	0.960	-	
$k=9$	0.879	-	0.895	-	0.800	-	0.969	-	
$k=9.5$	0.915	-	0.925	-	0.857	-	0.977	-	
$k=10$	0.936	-	0.945	-	0.894	-	0.978	-	

Model: $V(\varphi) = V_0 \left(\frac{\varphi}{M_p} \right)$			
Pan-Plus	Union3	DESY5	CMB
p_{null} N_{σ}	p_{null} N_{σ}	p_{null} N_{σ}	p_{null} N_{σ}
0.096 1.307	0.035 1.816	0.002 2.867	0.494 0.014

Model: $V(\varphi) = \frac{V_0}{2} \left(\frac{\varphi}{M_p} \right)^2$			
Pan-Plus	Union3	DESY5	CMB
p_{null} N_{σ}	p_{null} N_{σ}	p_{null} N_{σ}	p_{null} N_{σ}
0.097 1.296	0.037 1.791	0.002 2.847	0.502 -

Model: $V(\varphi) = \frac{V_0}{4} \left(\frac{\varphi}{M_p} \right)^4$			
Pan-Plus	Union3	DESY5	CMB
p_{null} N_{σ}	p_{null} N_{σ}	p_{null} N_{σ}	p_{null} N_{σ}
0.098 1.291	0.038 1.778	0.002 2.837	0.506 -

Model: $V(\varphi) = V_0 \exp\left(-\frac{k^2 \varphi^2}{2M_p^2}\right)$									
	Pan-Plus		Union3		DESY5		CMB		
	p_{null}	N_{σ}	p_{null}	N_{σ}	p_{null}	N_{σ}	p_{null}	N_{σ}	
$k=1$	0.092	1.326	0.034	1.823	0.002	2.875	0.490	0.025	
$k=1.2$	0.090	1.342	0.032	1.847	0.002	2.894	0.482	0.044	
$k=1.4$	0.087	1.360	0.031	1.873	0.002	2.915	0.473	0.067	
$k=1.5$	0.085	1.370	0.030	1.886	0.002	2.925	0.469	0.078	
$k=1.6$	0.084	1.379	0.029	1.900	0.002	2.937	0.464	0.091	
$k=1.8$	0.081	1.399	0.027	1.929	0.002	2.959	0.454	0.116	
$k=2$	0.078	1.419	0.025	1.959	0.001	2.983	0.443	0.143	
$k=2.5$	0.071	1.469	0.021	2.031	0.001	3.039	0.416	0.211	
$k=3$	0.065	1.515	0.018	2.099	0.001	3.090	0.391	0.276	
$k=3.5$	0.060	1.555	0.017	2.120	0.001	3.130	0.383	0.298	
$k=4$	0.059	1.560	0.028	1.904	0.001	2.985	0.430	0.177	
$k=4.5$	0.067	1.496	0.046	1.687	0.003	2.756	0.476	0.059	
$k=5$	0.103	1.263	0.097	1.299	0.011	2.298	0.567	-	
$k=5.5$	0.174	0.940	0.186	0.894	0.036	1.795	0.661	-	
$k=6$	0.263	0.633	0.290	0.552	0.086	1.366	0.736	-	
$k=6.5$	0.400	0.252	0.439	0.153	0.194	0.865	0.817	-	
$k=7$	0.537	-	0.577	-	0.332	0.433	0.869	-	
$k=7.5$	0.627	-	0.666	-	0.442	0.146	0.884	-	
$k=8$	0.730	-	0.759	-	0.577	-	0.925	-	
$k=8.5$	0.801	-	0.826	-	0.681	-	0.942	-	
$k=9$	0.863	-	0.881	-	0.781	-	0.947	-	
$k=9.5$	0.894	-	0.898	-	0.823	-	0.956	-	
$k=10$	0.928	-	0.937	-	0.891	-	0.963	-	

Model: $V(\varphi) = V_0 \left(1 + \frac{k^2 \varphi^2}{2M_p^2}\right)^{-1}$									
	Pan-Plus		Union3		DESY5		CMB		
	p_{null}	N_{σ}	p_{null}	N_{σ}	p_{null}	N_{σ}	p_{null}	N_{σ}	
$k=1$	0.128	1.136	0.104	1.258	0.011	2.302	0.608	-	
$k=2$	0.081	1.399	0.028	1.904	0.002	2.943	0.459	0.102	
$k=3$	0.066	1.503	0.019	2.067	0.001	3.068	0.401	0.250	
$k=4$	0.057	1.580	0.015	2.183	0.001	3.156	0.356	0.369	
$k=5$	0.052	1.628	0.016	2.147	0.001	3.178	0.363	0.350	
$k=6$	0.095	1.310	0.088	1.355	0.009	2.360	0.543	-	
$k=7$	0.300	0.525	0.327	0.449	0.111	1.219	0.718	-	
$k=8$	0.533	-	0.567	-	0.382	0.300	0.710	-	
$k=9$	0.720	-	0.745	-	0.645	-	0.809	-	
$k=10$	0.778	-	0.761	-	0.673	-	0.855	-	

Model: $V(\varphi) = V_0 \left(1 + \frac{k^2 \varphi^2}{M_p^2}\right)^{-1/2}$									
	Pan-Plus		Union3		DESY5		CMB		
	p_{null}	N_{σ}	p_{null}	N_{σ}	p_{null}	N_{σ}	p_{null}	N_{σ}	
$k=2$	0.085	1.371	0.038	1.778	0.002	2.861	0.491	0.023	
$k=3$	0.068	1.490	0.021	2.029	0.001	3.043	0.413	0.219	
$k=4$	0.058	1.571	0.015	2.160	0.001	3.141	0.364	0.348	
$k=5$	0.052	1.623	0.013	2.240	0.001	3.199	0.331	0.437	
$k=6$	0.049	1.656	0.011	2.288	0.001	3.235	0.309	0.499	
$k=7$	0.047	1.676	0.010	2.318	0.001	3.256	0.291	0.551	
$k=8$	0.046	1.689	0.010	2.339	0.001	3.270	0.269	0.615	
$k=9$	0.045	1.697	0.009	2.351	0.001	3.279	0.266	0.625	